Experimental methods.

General Methods. All reagents were commercial products and unless otherwise indicated they were used directly without any further purification. Tetrahydrofuran (THF), acetone and dichloromethane (DCM) were purchased from Beijing Tong Guang Fine Chemicals Company. THF was freshly distilled over sodium under nitrogen atmosphere prior to use. Acetone was used without further purification. ^{1}H NMR and ^{13}C NMR spectra were collected with Bruker ARX400 (400 MHz) instruments, using $CDCl_3$ as solvent. Chemical shifts are reported in parts per million (ppm) and coupling constants are reported in Hertz (Hz). ^{1}H and ^{13}C NMR chemical shifts were referenced to the residual solvent peak (7.26 ppm for ^{1}H and 77.0 ppm for ^{13}C). Electro-spray ionization (ESI) mass spectrometry was performed using a Bruker Apex IV FTMS instrument. 4-(5-Bromothiophen-2-yl)-7-(thiophen-2-yl)benzo[c][1,2,5]thiadiazole was synthesized according to the literature.[11]

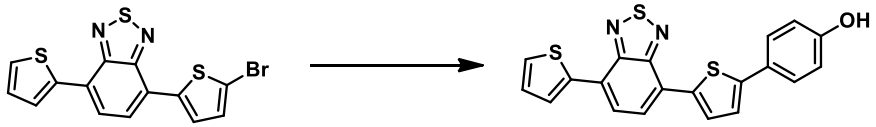

1

A 100 mL Schlenk tube was charged with 4-(5-Bromothiophen-2-yl)-7-(thiophen-2-yl)benzo[c][1,2,5]thiadiazole (1.39 g, 3.66 mmol), (4-Hydroxyphenyl)boronic acid (0.6 g, 4.35 mmol), $Pd(PPh_3)_4$ (0.17 g, 0.15 mmol). The tube was evacuated and refilled with nitrogen for 3 times. To the mixture was added degassed 1.7 M Na_2CO_3 (13 mL) and THF (39 mL) under nitrogen. The mixture was stirred at reflux for 12 h, then quenched with aqueous NH_4Cl. The aqueous layer was extracted by dichloromethane. The combined organic extract was washed with water and brine, dried over anhydrous $MgSO_4$, filtered and concentrated *in vacuo*. The solid residue was subjected to column chromatography (silica gel, petroleum ether/ethyl acetate, 2/1 v/v), 2/1 v/v) to get the product **1** (0.66 g, 57%) as a red powder. ^{1}H NMR (400 MHz, $CDCl_3$): δ 8.12 (d, 1H, J = 3.2 Hz), 8.10 (d, 1H, J = 3.2 Hz), 7.89 (d, 1H, J = 8.4 Hz), 7.87 (d, 1H, J = 8.4 Hz), 7.60 (d, 2H, J = 8.0 Hz), 7.46 (d, 1H, J = 4.8 Hz), 7.31-7.21 (m, 2H), 6.89 (d, 2H, J = 8.0 Hz). ESI-HRMS (m/z): $[M+H]^+$ calculated for $C_{20}H_{13}N_2OS_3^+$, 393.0185; found, 393.0185.

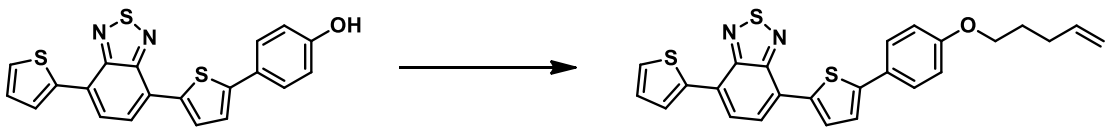

1 **2**

To an acetone solution (15 mL) of **1** (109 mg, 0.28 mmol) was added anhydrous K_2CO_3 (307 mg, 2.22 mmol), KI (23 mg, 0.14 mmol) and 5-bromo-1-pentene (124 mg, 0.83 mmol). The mixture was stirred at reflux overnight. After removal of acetone *in vacuo*, the residue was extracted by water. The aqueous phase was extracted repeatedly by dichloromethane. The organic extract was dried over anhydrous Na_2SO_4, filtered and concentrated *in vacuo*. The residue was subjected to flash column chromatography (silica gel, dichloromethane/petroleum ether, 1/3 v/v) to afford **2** (80 mg, 63%) as a red solid. ^{1}H NMR (400 MHz, $CDCl_3$): δ 8.12 (dd, 1H, J = 3.6 Hz, 0.8 Hz), 8.10 (d, 1H, J = 4.0 Hz), 7.89 (d, 1H, J = 8.0 Hz), 7.86 (d, 1H, J = 8.0 Hz), 7.63 (d, 2H, J = 8.4 Hz), 7.46 (dd, 1H, J = 4.8 Hz, 0.8 Hz), 7.31 (d, 1H, J = 4.0 Hz), 7.22 (dd, 1H, J = 4.8 Hz, 3.6 Hz), 6.94 (d, 2H, J = 8.4 Hz), 5.86 (m, 1H), 5.07 (m, 2H), 4.02 (t, 2H, J = 6.4 Hz), 2.27 (m, 2H), 1.92 (m, 2H). ^{13}C NMR (100 MHz, $CDCl_3$): δ 159.03, 152.66, 152.51, 145.70, 139.47, 137.77, 137.53, 128.70, 128.00, 127.51, 127.38, 127.09, 126.84, 126.80, 126.68, 126.02, 125.83, 125.56, 125.01, 122.99, 115.30, 114.94, 67.31, 30.12, 28.43. ESI-HRMS (m/z): $M^{\cdot+}$ calcd for $C_{25}H_{20}N_2OS_3^{\cdot+}$, 460.0732; found, 460.0742.

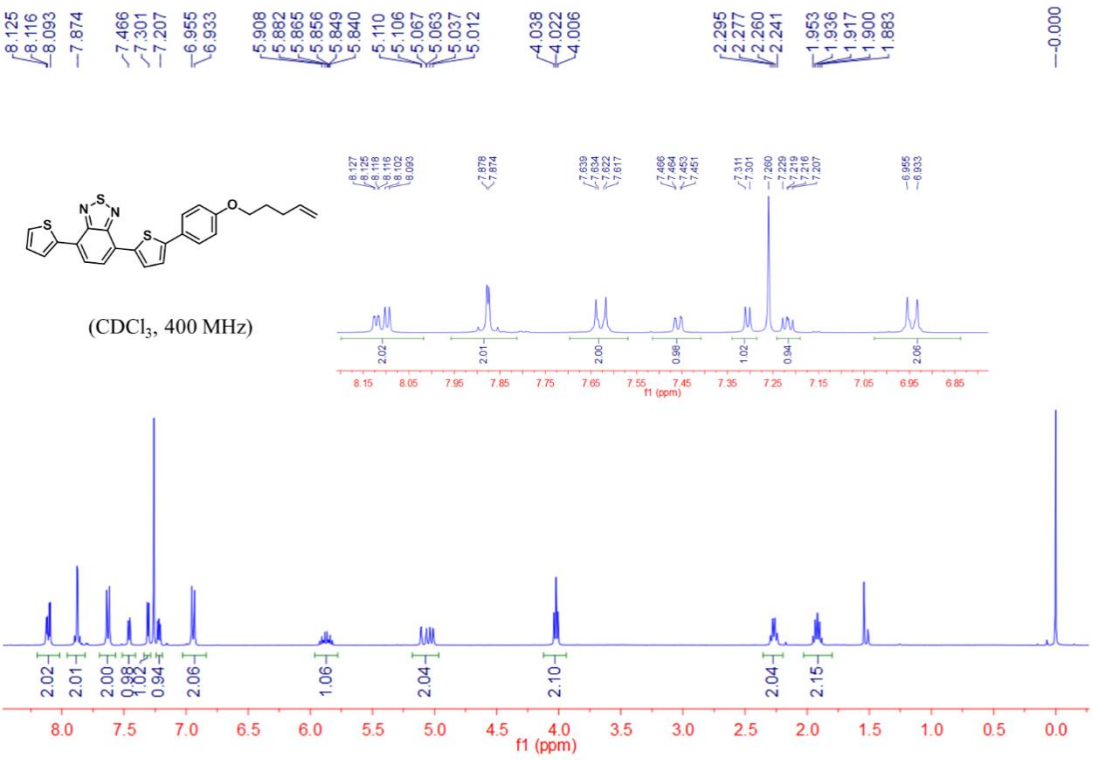

Figure S1. ^{1}H NMR spectrum of **2**

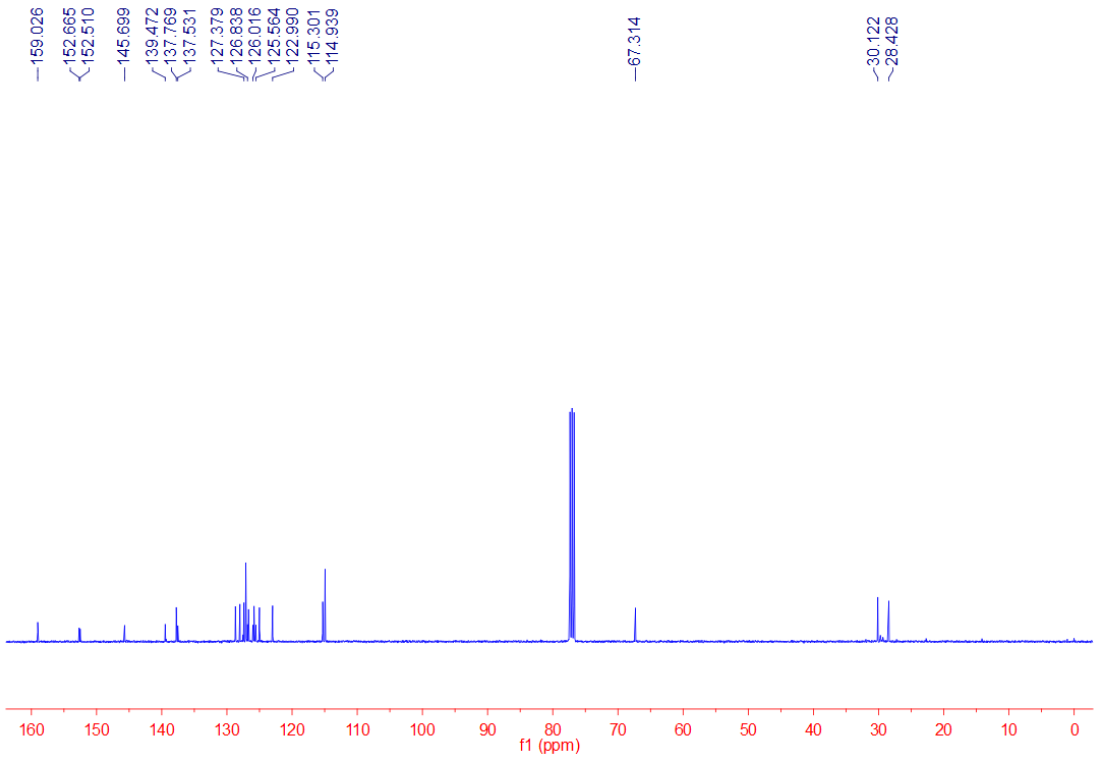

Figure S2. ^{13}C NMR spectrum of **2**

Synthesis and characterization of Si-TBT.

Silicon (Si) nanocrystals were synthesized through thermal decomposition of hydrogen silsesquioxane (HSQ). In a typical synthesis, 20 mL of Flowable Oxide (Fox-16, purchased from Dow Corning) was dried in the vacuum of a Schlenk Line for 6 hours, and the resulting white glassy powder was transferred to a quartz tube furnace and annealed at 1200°C in a 93% N_2 and 7% H_2 forming gas atmosphere for an hour, generating Si nanocrystals embedded in SiO_2 matrix. These SiO_2-embedded Si nanocrystals were ground with a pestle and mortar for 30 min and shaken with 3 mm borosilicate glass beads for 9 hours to yield a fine powder. Si nanocrystals were liberated by etching 300 mg of the fine powder with a mixture of 10 mL 48% hydrofluoric acid and 1 mL 37.5% hydrochloric acid in dark for 4 hours and collected by centrifuging at 8000 rpm for 5 min. Si nanocrystals were further rinsed once with DI water, twice with ethanol, once with chloroform, and finally dispersed in 5 mL of 1-dodecene. 200 mg of TBT was quickly added to the Si nanocrystal dispersion, which was sonicated for 1 min and transferred to a three-neck flask connected to a Schlenk line. The dispersion was degassed with three free-pump-thaw cycles and heated at 170°C in a N_2 gas environment for 12 hours to complete the functionalization of Si nanocrystals.

The Si nanocrystal 1-dodecene dispersion was cooled to room temperature and centrifuged at 8000 rpm for 5 min to precipitate uncapped/poorly capped nanocrystals. 15 mL of ethanol was added to the supernatant and the mixture was centrifuged at 8000 rpm for 5 min. The precipitate,

containing functionalized Si nanocrystals, was re-dispersed in 3 mL of toluene. These Si nanocrystals were cleaned five times by using toluene/ethanol as a solvent/anti-solvent pair, and finally dispersed in toluene at a concentration of 10 mg/mL.

Transmission electron microscopy images were acquired with a Tecnai Biotwin TEM operated at 80 kV accelerating voltage. Samples were made by drop casting 5 µL of toluene dispersion of TBT-Si nanocrystals at a concentration of 0.1 mg/mL onto carbon coated copper grids.

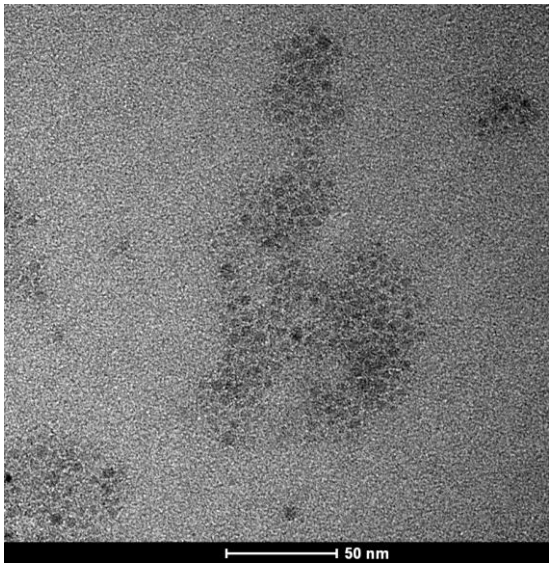

Figure S3. TEM image of 5 nm **Si-TBT**.

FTIR spectra were measured with a Bruker Vertex 70 FTIR depositing the samples on KBr plates from toluene solution.

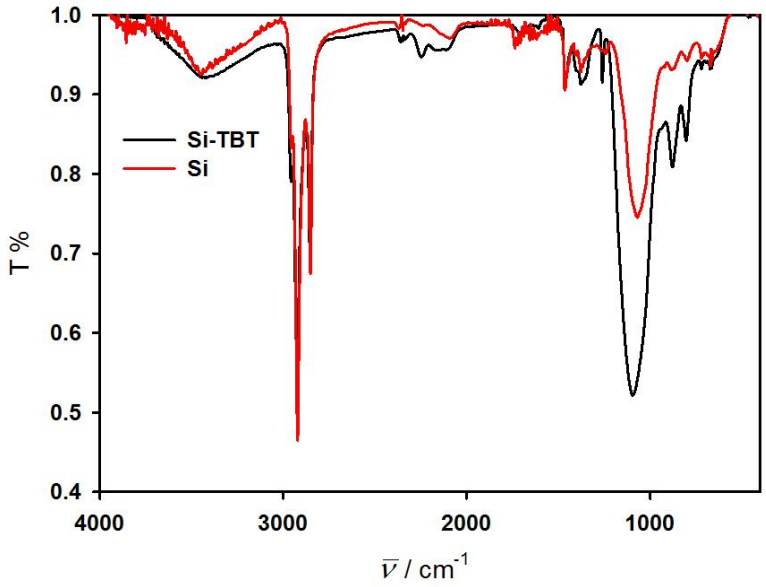

Figure S4. FTIR spectra of **Si** and **Si-TBT** of 5 nm diameter.

The FTIR spectrum of **Si** (red line, Figure S4) shows features of ν(C−H) stretching at 3000-2850 cm^{-1} and δ(C−H) bending at 1500-1350 cm^{-1}; the presence of the oxygen is evidenced by the strong ν(Si−O) stretching at 1080 cm^{-1}. The spectrum of **Si-TBT** (black line, Figure S4) is dominated by the silicon core and dodecyl chains; in both samples, there is no evidence of ν(Si-H) (ca. 2100 cm^{-1}) consistent with effective functionalization.

Computational details.

Quantum chemical calculations were carried out on **TBT** and on a symmetric model of **TBT** labelled **mTBT**. Atomic structures of **mTBT** and **TBT** were optimized with density functional theory (DFT) calculations using the CAM-B3LYP long range-corrected hybrid functional with the 6-31G** basis set. In general, time dependent (TD) DFT erroneously predicts the wrong order of charge transfer states and neutral states. For this reason, we run all the calculations employing the long-range corrected CAM-B3LYP functional.[2] The lowest energy conformer of both **TBT** and **mTBT** were considered in the calculations of the ground state properties. The geometry of the lowest excited state S_1 of **TBT** was also optimized with TDDFT/CAM-B3LYP calculations. In plotting the computed electronic absorption spectrum a Lorentzian line-width of 0.4 eV was superimposed to each computed intensity to facilitate the comparison with experimental spectra. The computed spectra did not include the vibronic structure associated with electronic bands. Because the TDDFT/CAM-B3LYP/6-31G** excitation energies are slightly overestimated compared with the experimental values, to facilitate comparison, the computed spectra were red shifted by 0.25 eV to match the first observed band. Molecular orbital shapes and energies discussed in the text are those calculated at the ground state optimized geometries. Orbital pictures were prepared with Molekel 4.3 visual software.[3] Geometry optimization of ground and excited states along with one photon absorption intensities were quantum-chemically computed with the Gaussian09 package.[4]
Two photon absorption activities were computed at TDDFT/CAM-B3LYP/6-31G** level of theory with the implementation[5] in the Dalton software package.[6] It has been shown that the CAM-B3LYP functional gives a description of two-photon absorption comparable to the coupled cluster model CC2.[7] The two-photon absorption strength for an average molecular orientation is computed in DALTON according to formulas given in refs. [8,9]. The absorption depends on the light polarization. A single linearly-polarized light source was assumed. A FWHM of 0.1 eV and a Lorentzian function is assumed in the calculation of two photon cross sections.[10]

Table S1. One photon and two photon absorption properties of **mTBT** from **TD-CAM-B3LYP/6-31G**** calculations.

Excited state	Energy/eV	$\sigma^{(2)}$ / GM[a]	f^b	Wavefunction composition
S_1	2.96	3	0.43	(H→L)
S_2	4.40	529	0.04	(H-1→L)
S_3	4.52	20	0.43	(H→L+1)

S_4	4.73	260	0.04	(H-1→L); (H-4→L)

[a]Two photon absorption cross-section for linearly polarized light (both photon with parallel polarization). [b]One photon oscillator strength.

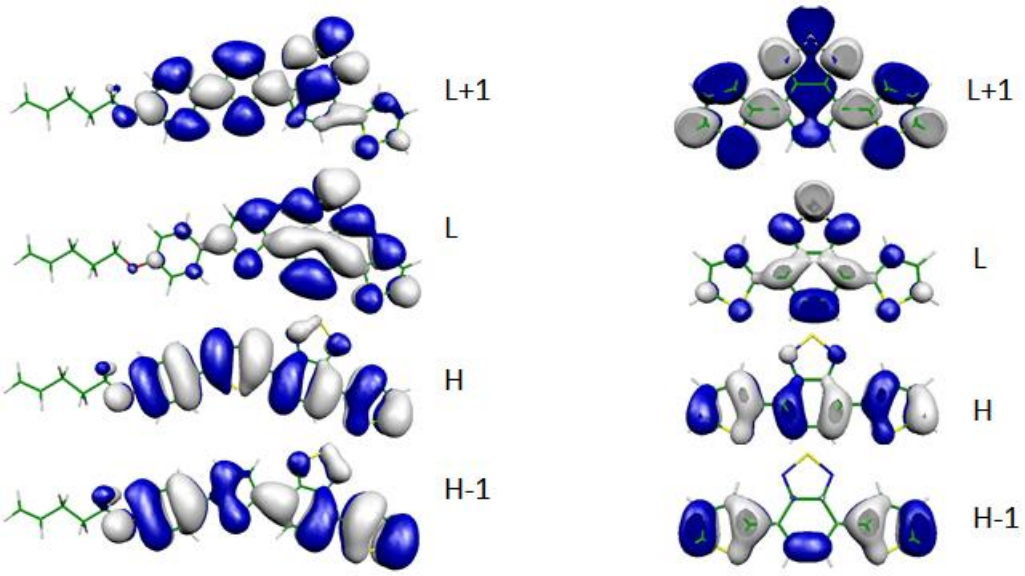

Figure S5. CAM-B3LYP/6-31G** frontier molecular orbitals of **TBT** (left) and **mTBT** (right) at the ground state optimized geometry.

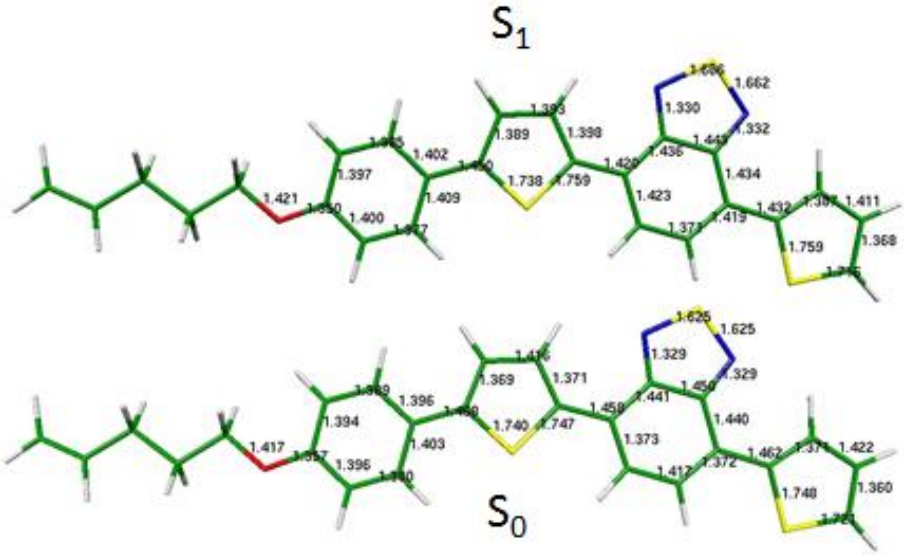

Figure S6. Equilibrium structures of the ground state (bottom) and lowest energy excited state (top) of **TBT** from CAM-B3LYP/6-31G** and TDDFT/CAM-B3LYP/6-31G** calculations, respectively.

Photophysical measurements.

Photophysical measurements were carried out in air-equilibrated solvents (hexanes, toluene, dichloromethane) at 298 K. UV-visible absorbance spectra were recorded with a Cary 300 UV/VIS spectrophotometer, using quartz cells with 1.0 cm path length.
Emission spectra were obtained with a Perkin Elmer LS-50 spectrofluorometer, equipped with a Hamamatsu R928 phototube, or an Edinburgh FLS920 spectrofluorometer equipped with a Ge-detector for emission in the NIR spectral region. Correction of the emission spectra for detector sensitivity in the 500-1200 nm spectral region was performed.
PL quantum yields were measured following the method of Demas and Crosby[11](standard used: 1,1',3,3,3',3'-hexamethylindotricarbocyanine iodide (HITCI) in ethanol for SiNCs and Rhodamine 6G in ethanol for **TBT**).[12]

PL lifetime measurements in the range 0.5 ns to 1 μs were performed by an Edinburgh FLS920 spectrofluorometer equipped with a TCC900 card for data acquisition in time-correlated single-photon counting experiments (0.2 ns time resolution) with a 340 nm pulsed diode and a LDH-P-C-405 pulsed diode laser.

PL lifetime measurements in the range 10 μs to 1 s were performed on a Perkin Elmer LS-50 spectrofluorometer equipped with a pulsed Xe lamp. The estimated experimental errors are: 2 nm on the band maximum, 5% on the molar absorption coefficient and luminescence lifetime, 10% on the fluorescence quantum yield.

Two-photon absorption (2PA) measurements. The 2PA spectra of TBT were recorded using the 2P excitation method and a setup described in detail previously.[13]

The emission spectra of rhodamine B (in MeOH)[1,2] and **TBT** in toluene obtained at different excitation wavelengths were used in calculations of the 2PA cross-sections. Typically, the average incident power on the sample was 100 mW (1.25 nJ/pulse). In this regime, the excited state population near the beam focus was well below saturation. The dependence of the emission intensity on the incident power at all excitation wavelengths was confirmed to be quadratic at powers up to 300 mW and above. When recording the emission images, CCD pixel intensities were kept approximately constant for all excitation wavelengths to avoid possible distortions due to the CCD non-linearity. Image intensities were adjusted by either tuning the laser power or the acquisition time, which was typically 10-30 s per image. The fs pulse duration (FWHM) varied in the range 160-125 fs in the wavelength range 700-1080 nm.

The comparison of emission of SiNC with and without the 2P antenna (**Si** vs **Si-TBT**) was performed in time-resolved fashion upon excitation of the samples by short (1-2 μs-long) trains of fs pulses (excitation gates) using a single PMT as a detector.[13]

Typically, 2,000-5,000 excitation gates were averaged to obtain the luminescence decays. The laser power was kept constant (typically 100 mW, i.e.1.25 nJ per pulse) when comparing samples of **Si** and **Si-TBT**. At 0.001 duty cycle (gate duration 1 □s, modulator rep. rate 1 kHz), the time-

averaged power on the sample was 0.1 mW. The resulting decays were normalized by the number of scans and the sample concentrations. The latter were determined spectrophotometrically from the linear absorption spectra.

Photophysical properties of TBT in solvents of different polarity.

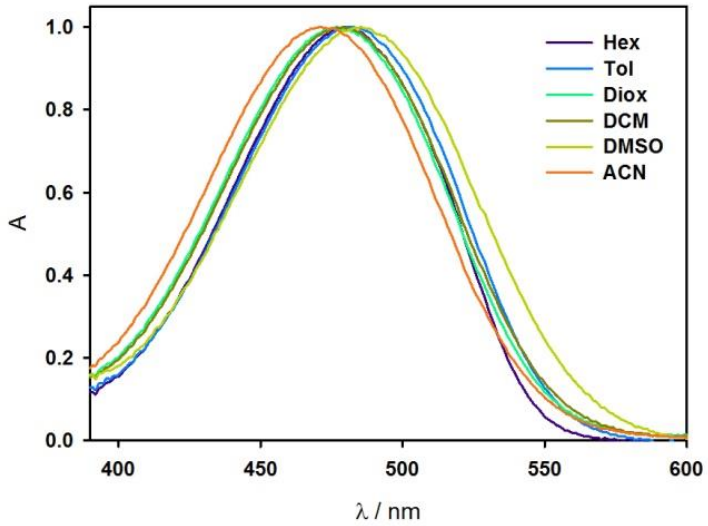

Figure S7. Absorption spectra of **TBT** in solvents of different polarity.

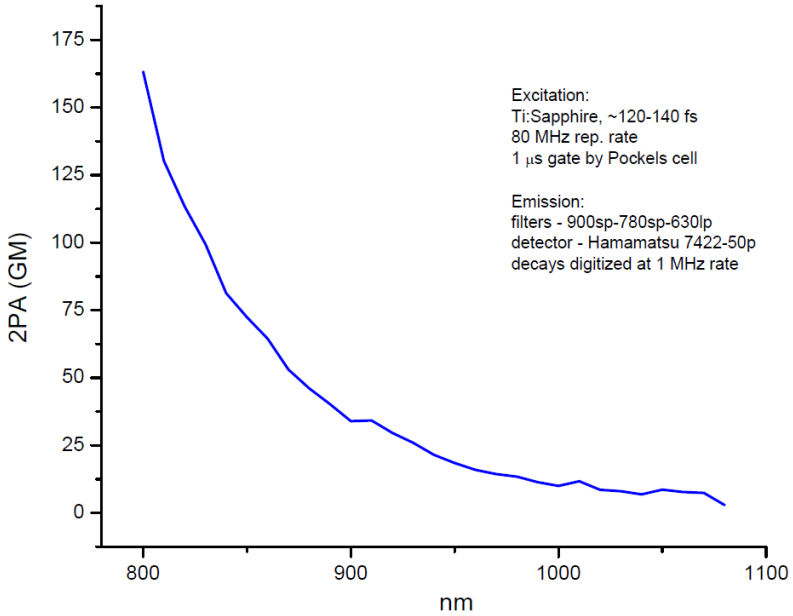

Figure S8. 2P absorption spectrum of dodecyl-capped SiNCs of diameter of 3 nm dispersed in hexane.

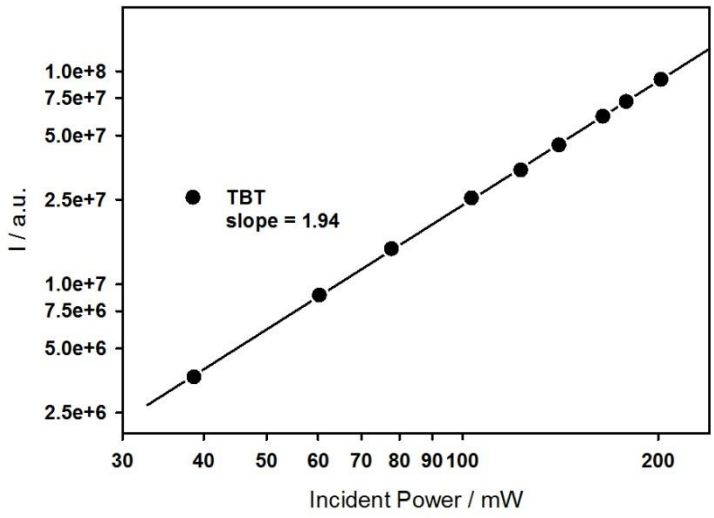

Figure S9. 2PA signal of **TBT** in toluene as a function of the laser incident power at 800 nm.

Photophysical properties of Si-TBT with a silicon core with an average diameter of 3 nm. In order to compare the photophysical properties as a function of the dimension of the silicon core, in the following we report the absorption and emission spectra (Figure S6) of a sample of SiNCs (average diameter of 3 nm) functionalized with dodecene and TBT (**Si_{3nm}-TBT**) in comparison to that functionalized only with dodecene (**Si_{3nm}**). Estimation of the energy transfer efficiency (35%) has been performed as reported in the following section.

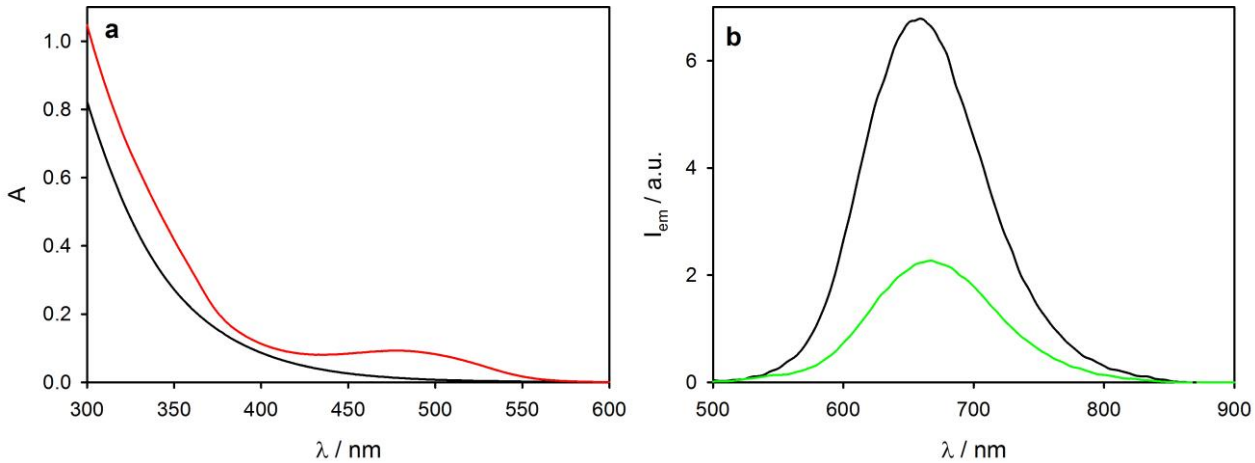

Figure S10. (a) Absorption spectra of **Si_{3nm}-TBT** (black line) and **Si_{3nm}** (red line) in toluene. (b) Emission spectrum of **Si_{3nm}-TBT** (black line) (λ_{ex}=480 nm) compared to that of an optically matched solution (at 480 nm) of **Si_{3nm}** and **TBT** (green line) in toluene.

Energy transfer efficiency in Si-TBT. To estimate the energy transfer efficiency, we performed emission spectra at two different excitation wavelengths:

- 390 nm, where **TBT** absorbance has a minimum: the absorbance of the **Si-TBT** sample is almost exclusively due to **Si** absorption (96% of light absorbed by **Si**(average diameter=5nm), 4% by **TBT**);
- 515 nm, near the maximum absorbance of **TBT**: the absorbance of the **Si-TBT** sample is mainly due to **TBT** (20% of light absorbed by **Si**(average diameter=5nm), 80% by **TBT**).

By keeping the experimental conditions constant and correcting for the different values of absorbance and incident photon flux at the two different wavelengths, it is possible to compare the emission intensities upon excitation at 390 nm (~100% **Si**) and 515 nm (80% **TBT**) to evaluate the amount of energy transfer from **TBT** to **Si**.

$I_{390,corr} = I_{390,exp} / ((1 - 10^{-A390}) * F_{390})$

$I_{515,corr} = I_{515,exp} / ((1 - 10^{-A515}) * F_{515})$

$\eta_{ET} = (I_{515,corr} * 0.8) / I_{390,corr}$

where $I_{\lambda,exp}$ and $I_{\lambda,corr}$ are the raw and corrected emission intensity upon excitation at wavelength λ, while A_λ and F_λ are the absorbance of the solution and the incident photon flux at wavelength λ (A_{390} = 0.071, A_{515} =0.031, F_{390} = 1.19x10^6 counts, F_{515} = 1.24x10^6 counts).

Energy transfer efficiency was calculated to be 75% in the case of **Si_{5nm}-TBT** (average diameter of the silicon core=5nm) and 35% in the case of **Si_{3nm}-TBT** (average diameter of the silicon core=3nm)

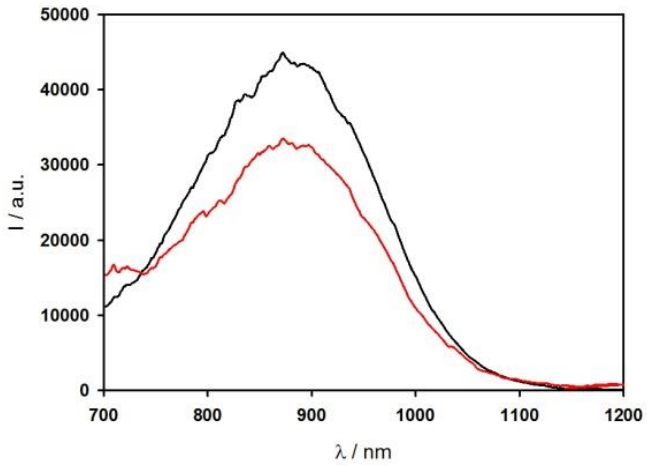

Figure S11. Corrected emission of **Si_{5nm}-TBT** upon excitation at 390 nm (black line) and 515 nm (red line) in toluene.

2P excitation of Si-TBT. Figure S12 reports a schematic diagram of the 2P antenna based **on Si-TBT**.

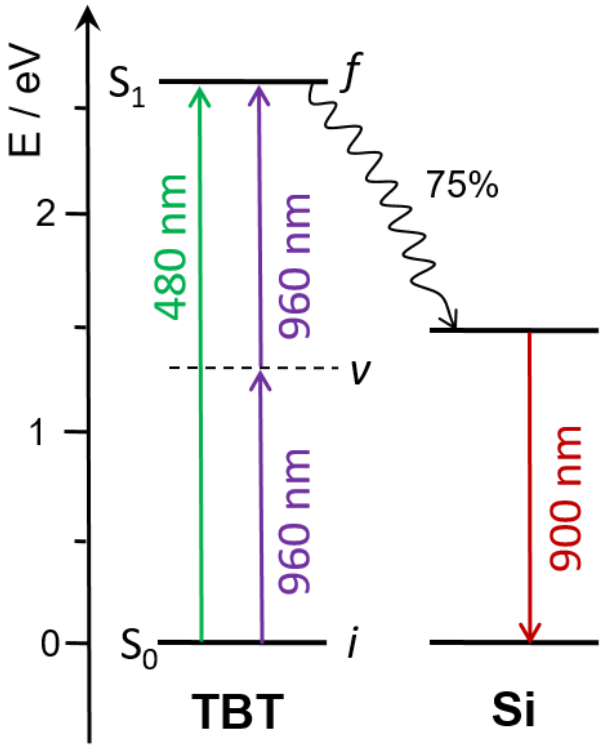

Figure S12. Schematic energy level diagram of the **TBT** chromophore and the Si core (average diameter = 5nm), evidencing energy transfer process by 1P (515 nm) and 2P (960 nm) excitation.

Two-photon transition to the lowest excited singlet state S_1 in TBT *via* the virtual state 'v' does not rely on resonances with any particular intermediate states 'p', since all these states are positioned above the final state S_1, and the corresponding detuning terms ($h\omega$-E_p) are relatively large. Instead, the transition is most likely due to a change in the static dipole moments between the initial ('i') state S_0 and the final ('f') state S_1.

References

[1] Z. Chen, E. M. Grumstrup, A. T. Gilligan, J. M. Papanikolas and K. S. Schanze, *J. Phy. Chem. B*, 2013, **118**, 372.

[2] Yanai, T.; Tew, D. P.; Handy, N. C. Chem. Phys. Lett. 2004, 393, 51-57.

[3] Molekel, version 4.3, http://www.cscs.ch/molekel/ ; Portmann, S.; Lüthi, H. P. *Chimia* **2000**, *54*, 766.

[4] Frisch, M. J.; Trucks, G. W.; Schlegel, H. B.; Scuseria, G. E.; Robb, M. A.; Cheeseman, J. R.; Scalmani, G.; Barone, V.; Mennucci, B.; Petersson, G. A.; et al. Gaussian 09, revision D.01; Gaussian, Inc.: Wallingford, CT, 2009.

[5] P. Salek, O. Vahtras, J. Guo, Y. Luo, T. Helgaker, H. Ågren, Chem. Phys. Lett., 2003, 374, 446–452.

[6] K. Aidas, C. Angeli, K. L. Bak, V. Bakken, R. Bast, L. Boman, O. Christiansen, R. Cimiraglia, S. Coriani, P. Dahle, E. K. Dalskov, U. Ekstro¨m, T. Enevoldsen, J. J. Eriksen, P. Ettenhuber, B. Ferna´ndez, L. Ferrighi, H. Fliegl, L. Frediani, K. Hald, A. Halkier, C. Ha¨ttig, H. Heiberg, T. Helgaker, A. C. Hennum, H. Hettema, E. Hjertenæs, S. Høst, I.-M. Høyvik, M. F. Iozzi, B. Jansi´k, H. J. Aa. Jensen, D. Jonsson, P. Jørgensen, J. Kauczor, S. Kirpekar, T. Kjærgaard, W. Klopper, S. Knecht, R. Kobayashi, H. Koch, J. Kongsted, A. Krapp, K. Kristensen, A. Ligabue, O. B. Lutnæs, J. I. Melo, K. V. Mikkelsen, R. H. Myhre, C. Neiss, C. B. Nielsen, P. Norman, J. Olsen, J. M. H. Olsen, A. Osted, M. J. Packer, F. Pawlowski, T. B. Pedersen, P. F. Provasi, S. Reine, Z. Rinkevicius, T. A. Ruden, K. Ruud, V. Rybkin, P. Salek, C. C. M. Samson, A. S. de Mera´s, T. Saue, S. P. A. Sauer, B. Schimmelpfennig, K. Sneskov, A. H. Steindal, K. O. Sylvester-Hvid, P. R. Taylor, A. M. Teale, E. I. Tellgren, D. P. Tew, A. J. Thorvaldsen, L. Thøgersen, O. Vahtras, M. A. Watson, D. J. D. Wilson, M. Ziolkowski and H. Ågren, Wiley Interdiscip. Rev.: *Comput. Mol. Sci.*,**2014**,*4*, 269–284.

[7] D. H. Friese, C. Hättig, K. Ruud, *Phys. Chem. Chem. Phys.* **2012**, *14*, 1175-1184

[8] P.R. Monson, W.M. McClain, *J. Chem. Phys.* **1970**, *53*, 29.

[9] W.M. McClain, *J. Chem. Phys.* **1971**, *55*, 2789.

[10] D. H. Friese, M. T. P. Beerepoot, M. Ringholm, K. Ruud, *J. Chem. Theory Comput.* **2015**, *11*, 1129-1144

[11]J.N. Demas, G.A. Crosby, *J. Phys. Chem.* **1971**, *75*, 991-1024.

[12] (a) C. Würth, J. Pauli, C. Lochmann, M. Spieles, U.; Resch-Genger, *Anal. Chem.* **2012**, *84*, 1345-1352. (b) C. Würth, M. Grabolle, J. Pauli, M. Spieles, U. Resch-Genger, *Nature Prot.* **2013**, *8*, 1535-1550.

[13] T. V. Esipova, H. J. Rivera-Jacquez, B. Weber, A. E. Masunov, S. A. Vinogradov, *J. Am. Chem. Soc.* **2016**, *138*, 15648−15662.